Colloidal Assembly

DOI: 10.1002/anie.200805204

A Microfluidic Approach to Chemically Driven Assembly of Colloidal Particles at Gas–Liquid Interfaces**

*Jai Il Park, Zhihong Nie, Alexander Kumachev, Ahmed I. Abdelrahman, Bernard P. Binks, Howard A. Stone, and Eugenia Kumacheva**

Colloidal particles with appropriate wettability strongly adsorb at liquid–gas interfaces and thereby act as efficient bubble stabilizers.[1–7] Bubbles that are encapsulated by a close-packed monolayer of solid particles (armored bubbles) have an extremely high stability toward coalescence, the ability to acquire anisotropic shapes, and the capability to suppress the dissolution of the trapped gas.[1–5] These properties make armored bubbles useful for the fabrication of thermal and acoustic insulators, and lightweight materials with high structural stability.[6–10]

Currently, the production of armored bubbles relies on injection methods or the shear of a mixture of two immiscible fluids.[2,4–7] These methods generate polydisperse bubbles in an uncontrollable manner, thus precluding the fabrication of materials with hierarchical periodic structures and related interesting optical and mechanical properties. Recently, hydrodynamic flow was used for the controlled assembly of colloidal particles at gas–liquid interfaces.[3] The strategy relied on the shear-assisted delivery of particles to the gas surface and the productivity of the method was approximately 10 bubbles per second.

Herein, we report an efficient strategy, which uses local perturbations of pH on the length scale of an individual bubble, for the continuous, single-step production of armored bubbles with a predetermined size, narrow polydispersity, and high productivity. Our method yields armored bubbles with polydispersity below 5% and a productivity of up to 3000 bubbles per second. The generality of the strategy is demonstrated by the ability to control the size of the encapsulated bubbles and by coating the bubbles with a variety of colloidal particles. The described approach provides a new route to the fabrication of materials with advanced properties such as optical resonators, three-dimensional foams with ordered structures, and ultra-light two-dimensional coatings with controlled pore sizes.

The proposed approach employs the following steps: 1) the microfluidic generation of monodisperse CO_2 bubbles in an aqueous dispersion of anionic colloidal particles, 2) the rapid dissolution of CO_2, which results in the shrinkage of the bubbles and an increase in the acidity of the solution in the neighborhood of the bubbles, and 3) the adsorption of the particles at the gas–liquid interface, the process being driven by the chemically induced in situ change in the surface energy of the particles. We used a planar microfluidic T-junction device to produce plugs of CO_2 in an aqueous dispersion of anionic polymer particles (Figure 1a).[11] A dispersion of poly(styrene-*co*-acrylic acid) (PS-*co*-PAA) particles in an aqueous NaOH solution was supplied to the main channel at a typical flow rate Q_L ranging from 7.5 to 24 mL h^{-1}, and

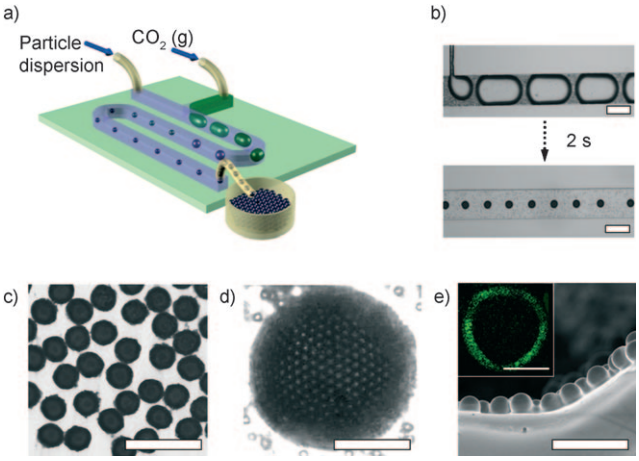

Figure 1. Continuous microfluidic generation of armored bubbles by dissolving CO_2. a) A schematic drawing of a microfluidic T-junction bubble generator. The widths of the main and the side channels are 220 and 40 μm, respectively. The height of the channels is 130 μm. b) Optical microscopy images of the CO_2 plugs generated at 28 °C, pH 14, P_{CO_2} = 5 psi, Q_L = 10.5 mL h^{-1}, and particle concentration C_p = 1.5 wt% (top); progression of the plugs to spherical armored bubbles, within 2 s after their formation, at a distance of 150 mm from the T-junction (bottom). c, d) Optical microscopy images of armored bubbles generated as in (b) and collected at the outlet of the microfluidic device. Scale bars: 200 μm (b, c) and 25 μm (d). e) SEM image (side view) of the shell of the microtomed armored bubble infiltrated with poly(ethylene glycol) diacrylate. Scale bar: 10 μm. The inset shows a CFM image of the bubble coated with HY-labeled PS-*co*-PAA particles (scale bar: 25 μm).

[*] J. I. Park,[+] Dr. Z. H. Nie,[+] A. Kumachev, A. I. Abdelrahman, Prof. Dr. E. Kumacheva
Department of Chemistry, University of Toronto
80 Saint George Street, Toronto M5S 3H6, Ontario (Canada)
Fax: (+1) 416-978-3576
E-mail: ekumache@chem.utoronto.ca
Prof. Dr. B. P. Binks
Surfactant and Colloid Group, Department of Chemistry
University of Hull, Hull, HU6 7RX (UK)
Prof. Dr. H. A. Stone
School of Engineering and Applied Sciences, Harvard University
Cambridge, MA 02138 (USA)
[+] These authors contributed equally to this work.

[**] E.K. thanks the Canada Research Chair (NSERC Canada) for financial support of this work. A. Petukhova and I. Gorelikov are thanked for assistance in the synthesis of cationic particles and CdSe/ZnS core–shell quantum dots.
Supporting information for this article is available on the WWW under http://dx.doi.org/10.1002/anie.200805204.

gaseous CO_2 (99.8%, BOC Canada) was introduced into the orthogonal channel. The CO_2 thread periodically broke up to release gaseous plugs with a polydispersity of 2–5%, which, owing to the dissolution of CO_2, underwent a dramatic decrease in volume and acquired a spherical shape (Figure 1b).[12]

Figure 1c shows a typical image of the bubbles collected at the outlet of the microfluidic device. A uniform dissolution and mass transfer achieved in the microchannels yielded armored bubbles with a narrow size distribution. The particles formed a close-packed two-dimensional crystalline shell on the bubble surface (Figure 1d). Imaging of microtomed bubbles by using SEM confirmed that the particles formed a monolayer-thick shell (Figure 1e). Labeling of the polymer particles with the fluorescent dye Hostasol Yellow (HY) allowed visualization of the colloidal shell by using confocal fluorescence microscopy (CFM; Figure 1e, inset).

The armored bubbles were stable toward coalescence and disproportionation, and had a narrow polydispersity of 2–5%. The approximate generation frequency of the armored bubbles was up to 700 bubbles per second, however, the productivity of the method was increased to around 3000 bubbles per second by using a microfluidic flow-focusing bubble generator (see Figure S1 in the Supporting Information).[13]

We also conducted a series of control experiments (Figure 2). In a particle-free environment at pH 14, the

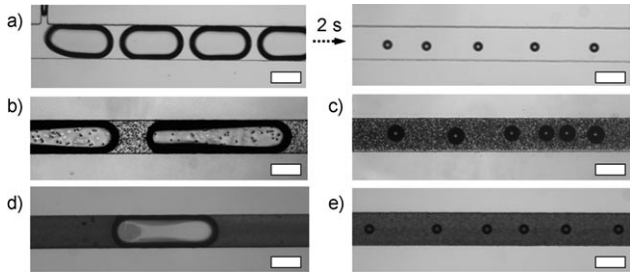

Figure 2. Optical microscopy images of bubbles and plugs flowing through the microchannels. a) Dissolution of CO_2 plugs in particle-free aqueous NaOH solution at pH 14. b) Plugs of gaseous N_2 formed in a dispersion of anionic PS-*co*-PAA particles. c) Bubbles of CO_2 generated in a dispersion of PS-*co*-PAA particles containing 2 wt% of the non-ionic surfactant TX-100. d) Plugs of N_2 formed in a dispersion of 700 nm diameter cationic PMMA-*co*-PVP particles. e) Bubbles of CO_2 dispersed in an aqueous dispersion of 700 nm diameter PMMA-*co*-PVP particles. In all experiments $Q_L = 10.5\ mL\,h^{-1}$, $C_p = 1.5$ wt%, pH 14, and $P_{CO_2} = 5$ psi. Scale bar: 200 μm.

shrinkage of CO_2 plugs was similar to that shown in Figure 1b, which suggests that, at this pH value, the size of the bubbles was determined by the dissolution of CO_2 and not the formation of the colloidal shell (Figure 2a). The role of CO_2 and the carboxylation of microbeads was established by showing that the armored bubbles did not form in experiments conducted with PS-*co*-PAA particles and N_2 bubbles (Figure 2b), or with PS-*co*-PAA particles and CO_2 bubbles in the presence of surfactants (Figure 2c). The surfactants changed a delicate balance in the wetting angles of the particles and the gas–liquid interface. Cationic poly(methyl methacrylate-*co*-vinyl pyridine) (PMMA-*co*-PVP) beads loosely covered negatively charged N_2 and CO_2 bubbles (Figure 2d and e, respectively),[14] which were prone to coalescence and acquired a broad size distribution when collected at the outlet of the device.

We explain the formation of armored bubbles as follows. The dissolution of CO_2 was followed by the reaction $CO_2 + 2\,OH^- \rightleftharpoons CO_3^{2-} + H_2O$, which, when the pH value is equal to or greater than 10, is dominated by the step $CO_2 + OH^- \rightleftharpoons HCO_3^-$.[12] Consequently, this reaction led to a local decrease in the pH of the liquid adjacent to the bubble surface, which caused the protonation of the carboxylic groups on the surface of the particles and an increase of the wetting angle θ of water on the polymer surface (Figure 3a).

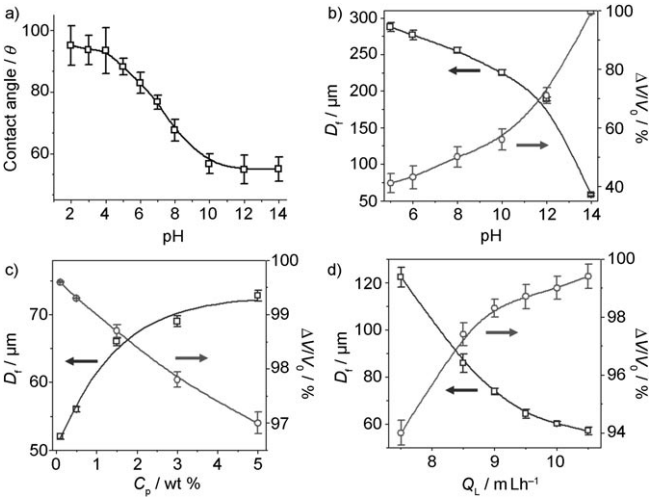

Figure 3. a) Variation in contact angle of an aqueous solution of NaOH in air on the PS-*co*-PAA film, measured at different pH values. b–d) Effect of experimental variables on the final diameter D_f of armored bubbles (□) and on the fractional change in volume of the CO_2 plugs (○). b) Effect of initial pH value of the continuous phase at $P_{CO_2} = 4.5$ psi, $C_p = 1.5$ wt%, $Q_L = 9.5\ mL\,h^{-1}$. c) Effect of C_p at $P_{CO_2} = 5$ psi, pH 14, $Q_L = 10.0\ mL\,h^{-1}$. d) Effect of the flow rate Q_L of the continuous phase, $P_{CO_2} = 5$ psi, pH 14, $C_p = 1.5$ wt%.

The protonation of the carboxylic groups on the particle surface in the region with reduced pH-favored adsorption of the microbeads on the bubbles. The particles adsorbed at a gas–liquid interface with a surface-energy reduction $E = \pi a^2 \gamma_{G,L}(1 \pm \cos\theta)^2$, where $\gamma_{G,L}$ is the interfacial tension of the gas–liquid interface and a is the radius of the particles.[15] We stress that the particles were hydrophobized only in the vicinity of the bubbles. In the rest of the continuous phase, mixing led to the equalization of the concentration of HCO_3^-, and the particles retained their colloidal stability. This feature favorably contrasts our approach to previous methods producing particle-stabilized foams, which involved the application of an external stimulus to the entire system and thereby compromised the stability of the particles in the dispersion.[16]

The final diameter D_f of the armored bubbles was controlled by several experimental variables (Figure 3). Figure 3b shows the effect of the original pH value of the continuous phase on the final diameter D_f of the bubbles and the fractional change in volume $\Delta V/V_0$ of gaseous plugs at a

particle concentration C_p of 1.5 wt% (V_0 and ΔV are the initial volume and the change in volume of the plugs, respectively; see also Figure S2 in the Supporting Information). As the pH value increased, a more rapid dissolution of CO_2 yielded smaller bubbles that were uniformly covered with particles. At pH 14, the value of $\Delta V/V_0$ reached 99.5%. In the experiments conducted at pH 14 in a particle-free environment, the CO_2 plugs underwent a similar 99.5% change in volume, which suggests that, at this pH value, the size of bubbles was not affected by particle adsorption. The concentration of dissolved CO_2 in the water phase was 0.02 mol L^{-1}, that is, the system was far from the saturation concentration of 1.03 mol L^{-1} (see the Supporting Information).[12,17] Thus, we conclude that the final volume of the bubbles was determined by the remaining inert gas. When the pH was less than 10, the bubbles retained their pluglike shape and were only partly covered with particles, because of the substantially slower dissolution of CO_2 than at pH 14.[12] Owing to the incomplete coverage with microbeads, these plugs were prone to coalescence and, when collected at the outlet, they formed large, nonspherical armored bubbles (see Figure S2 in the Supporting Information). Figure 3c shows that the final diameter of the armored bubbles increased with an increasing value of C_p (the initial dimensions of the CO_2 plugs did not depend on the value of C_p). Rapid formation of the colloidal shell counteracted the shrinkage of the plugs, thereby providing additional control over the size of the armored bubbles. For the concentration of particles in the range 1 wt% $< C_p <$ 5 wt% (1 wt% $= 4.3 \times 10^8$ particles mL^{-1}), the colloidal armor suppressed coalescence of the bubbles, whose polydispersity remained below 5%. When the C_p value was less than 1 wt%, the bubbles were poorly covered with particles and coalesced at the outlet of the microfluidic device to form large armored bubbles with a broad size distribution (see Figure S3 in the Supporting Information).

Figure 3d shows the effect of the flow rate of the continuous phase Q_L on the final diameter of the armored bubbles at pH 14. As the Q_L value increased, the final diameter of the armored bubbles decreased (see also Figure S4 in the Supporting Information). This effect occurred because of the generation of smaller gaseous plugs and a more efficient dissolution of CO_2 achieved at high values of Q_L.[18] At the largest values of Q_L, the fractional reduction in volume $\Delta V/V_0$ of the plugs reached 99.5%, that is, almost all the CO_2 left the plugs.

We developed a model that rationalizes our observations and accounts for the shrinkage of bubbles and the adsorption of particles to the gas–liquid interface. These two processes are coupled: dissolution of CO_2 occurs only through uncovered regions of the gas–liquid interface. For a bubble of radius $R_b(t)$ and the number of adsorbed particles $n_p(t)$, the uncovered bubble area is $(4\pi R_b(t)^2 - \alpha\pi a^2 n_p(t))$ where α depends on the contact angle. The two evolution equations have the form [Eq. (1)]

$$\frac{dR_b(t)^3}{dt} = -q_b(4\pi R_b(t)^2 - \beta\alpha\pi a^2 n_p(t))$$
$$\frac{dn_p(t)}{dt} = q_p(4\pi R_b(t)^2 - \alpha\pi a^2 n_p(t)) \quad (1)$$

where the constant $\beta \approx 1$ accounts for the elimination of CO_2 dissolution once the particles are close-packed.[9] The gas and particle fluxes, q_b and q_p, respectively, depend on the speed U and the radius of the bubble. For large Peclet numbers, $UR_b(t)/D \gg 1$, where D is the respective diffusion coefficient, we expect the values of q_b and q_p to scale similarly with U and $R_b(t)$. For such transport processes, q_p is proportional to C_p, which is analogous to Fick's law. The bubbles shrink faster when the pH is higher, since the diffusion of dissolved CO_2 in the liquid boundary layer is accompanied by the reaction with OH^- ions. Thus, we expect the value q_b to increase with increasing pH value. When the weak dependence on β is neglected, the ratio of the two equations yields [Eq. (2)]

$$\frac{dR_b(t)^3}{dn_p(t)} = -B \quad (2)$$

where the value of B is practically constant at fixed pH and C_p values but decreases as the C_p value increases, and increases as the pH value increases. Thus, for the initial condition $R_b(0) = R_0$ and $n_p(0) = 0$, the equilibrium bubble radius R_{eq} satisfies the equation [Eq. (3)]

$$\frac{R_0^3 - R_{eq}^3}{R_{eq}^2} = \frac{4B}{a^2} \quad (3)$$

that is, the R_{eq} value decreases monotonically as the B value increases. Given the characterization of B above, we conclude that the bubble radius increases as the particle concentration C_p increases, which is consistent with our observations (Figure 3c). Also, since faster gas dissolution (increasing B value) occurs at high pH values because of the simultaneous CO_2 diffusion and the reaction with OH^- ions, we conclude that the bubble radius decreases as the pH increases, which is in agreement with the experimental trends shown in Figure 3d.

The generality of our approach to armored bubbles was exemplified by coating the bubbles with different types of anionic particles and mixtures thereof. Figure 4 shows bubbles encapsulated by a mixture of HY-labeled and dye-free PS-*co*-PAA microspheres of similar dimensions (Figure 4a), carboxylated silica particles (Figure 4b), a mixture of carboxylated silica particles and HY-labeled PS-*co*-PAA, and 20 nm diameter carboxylated silica nanoparticles loaded with CdSe/ZnS core–shell quantum dots (QDs; Figure 4c).

We also encapsulated bubbles with the protein bovine serum albumin labeled with fluorescein isothiocyanate (FITC–BSA), which was dissolved in an aqueous phase at pH 7. Following the dissolution of CO_2, the bubbles were coated with 1–2 μm sized protein in size (Figure 4d). We believe that this observation indicates that, in the acidic environment adjacent to the shrinking bubbles, the protein molecules reached their isoelectric point of pH 4.8 and aggregated to form clusters that precipitate on the bubble surface.[19]

In summary, our strategy for the chemically mediated generation of armored bubbles maintains the high colloidal stability of particles in bulk materials, increases productivity, and can be used to form bubbles with precisely controlled

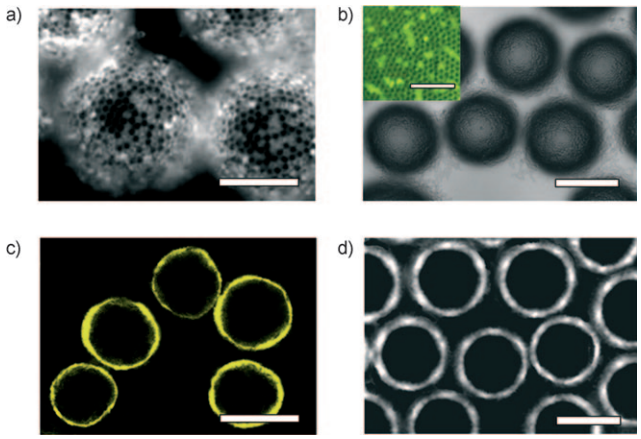

Figure 4. Generation of bubbles with various types of colloidal armor. a) Fluorescence microscopy image of bubbles coated with a close-packed shell of 2.8 μm diameter HY-labeled PS-*co*-PAA particles ($C_p = 0.5$ wt%) and 3.5 μm diameter PS-*co*-PAA particles ($C_p = 1.0$ wt%), $P_{CO_2} = 6$ psi, $Q_L = 12$ mL h^{-1}, pH 14. Scale bar: 50 μm. b) Optical microscopy image of bubbles coated with 3 μm diameter carboxylated silica particles. $P_{CO_2} = 12$ psi, $Q_L = 24$ mL h^{-1}, pH 14, and $C_p = 1.5$ wt%. Scale bar: 100 μm. The inset shows a fluorescence microscopy image of the surface of an armored bubble coated with 3 μm diameter carboxylated silica particles and 2.8 μm diameter HY-labeled PS-*co*-PAA polymer particles in the continuous phase in the weight ratio 3:1, respectively. Scale bar: 25 μm. c) CFM image of bubbles encapsulated with 20 nm diameter carboxylated silica nanoparticles loaded with CdSe/ZnS QDs, $\lambda_{exc} = 480$ nm. $P_{CO_2} = 8$ psi, $Q_L = 23$ mL h^{-1}, pH 10, and $C_p = 0.12$ wt%. Scale bar: 100 μm. d) Fluorescence microscopy image of armored bubbles engulfed with the FITC–BSA shell, $\lambda_{exc} = 495$ nm. The bubbles were generated at $P_{CO_2} = 6.5$ psi, $Q_L = 13$ mL h^{-1}, pH 7, and a protein concentration of 0.02 wt%. Scale bar: 100 μm.

dimensions. The armored bubbles generated by using the proposed strategy have potential applications in the production of three-dimensional foams with hierarchical order and ultralight two-dimensional coatings with precisely controlled pore sizes, for use as ultrasonic and magnetic resonance imaging (MRI) contrast agents, aerated food, and optical resonators. Furthermore, the generation of small bubbles is usually either expensive,[20] or it lacks control over bubble size distribution. By using the described approach, these problems can be solved by 1) producing large monodisperse bubbles from gaseous mixtures and 2) controllably removing one of the components of the mixture to reach the targeted bubble size.

The described strategy can be expanded in several ways. The deposition of cationic particles can be achieved by dissolving, for example, NH_3 and increasing the pH in the region adjacent to the surface of the bubbles. An increase in the productivity of the process can be achieved by using parallel integrated microfluidic bubble generators.[21,22] Controllable transfer of one of the components of the gaseous mixture to the continuous phase would provide the ability to control the composition of the bubbles and the surrounding medium, and activate a particular reaction on demand.

Experimental Section

Photolithographic masters were prepared using SU-8 50 photoresist (MicroChem) in bas relief on silicon wafers. The microfluidic devices were fabricated in PDMS by using a standard soft lithography procedure.[23] The CO_2 gas was supplied to the microfluidic device through polytetrafluoroethylene tubing (Small Parts, USA) attached to the Bellofram pressure regulator. The continuous phase was introduced into the device using a syringe pump (Harvard Apparatus, USA, PHD 2000 series). An Olympus BX51 microscope and a high-speed camera (Photometrics CoolSNAP ES) were used to acquire optical microscopy images. Image Pro (Media Cybernetics) software was used to determine the size of the bubbles. The volume of the spherical armored bubbles was calculated as $V_{sp} = 4/3\pi(D_f/2)^3$ where D_f is the diameter of armored bubble. The size distribution of the bubbles was characterized by the coefficient of variation as $CV(\%) = (\sigma/D) \times 100$, where D is the mean diameter of the bubbles and σ is the standard deviation of the bubble diameter. When the unperturbed diameter D of the bubbles (determined as $D = (6V/\pi)^{1/3}$ where V is the volume of the bubbles) was larger than the dimensions of the microchannel, they acquired the shape of a plug, as shown in Figure 1b. The effective final diameter (D_f) of the gaseous plugs was calculated as $D_f = 2(3V_{plug}/4\pi)^{1/3} = 2(3Ah/4\pi)^{1/3}$ where A is the area of a bubble and h is the height of a microchannel. Advancing contact angles between the spin-coated PS-*co*-PAA film and an aqueous solution of NaOH were measured in air at different pH values by using a droplet shape analyzer (DSA100, Krüss). The syntheses of polymer particles and silica-encapsulated quantum dots are described in the Supporting Information.

Received: October 23, 2008
Revised: February 13, 2009
Published online: March 19, 2009

Keywords: colloids · interfaces · microfluidics · self-assembly · surface chemistry

[1] A. R. Studart, U. T. Gonzenbach, I. Akartuna, E. Tervoort, L. J. Gauckler, *J. Mater. Chem.* **2007**, *17*, 3283.
[2] B. P. Binks, T. S. Horozov, *Angew. Chem.* **2005**, *117*, 3788; *Angew. Chem. Int. Ed.* **2005**, *44*, 3722.
[3] A. B. Subramaniam, M. Abkarian, H. A. Stone, *Nat. Mater.* **2005**, *4*, 553.
[4] U. T. Gonzenbach, A. R. Studart, E. Tervoort, L. J. Gauckler, *Angew. Chem.* **2006**, *118*, 3606; *Angew. Chem. Int. Ed.* **2006**, *45*, 3526.
[5] S. Fujii, A. J. Ryan, S. P. Armes, *J. Am. Chem. Soc.* **2006**, *128*, 7882.
[6] B. P. Binks, R. Murakami, *Nat. Mater.* **2006**, *5*, 865.
[7] R. G. Alargova, D. S. Warhadpande, V. N. Paunov, O. D. Velev, *Langmuir* **2004**, *20*, 10371.
[8] *Cellular Ceramics: Structure, Manufacturing, Properties and Applications* (Eds.: M. Scheffler, P. Colombo), Wiley-VCH, Weinheim, **2005**.
[9] M. Abkarian, A. B. Subramaniam, S. H. Kim, R. J. Larsen, S. M. Yang, H. A. Stone, *Phys. Rev. Lett.* **2007**, *99*, 188301.
[10] A. Bala Subramaniam, M. Abkarian, L. Mahadevan, H. A. Stone, *Nature* **2005**, *438*, 930.
[11] T. Thorsen, R. W. Roberts, F. H. Arnold, S. R. Quake, *Phys. Rev. Lett.* **2001**, *86*, 4163.
[12] P. V. Danckwerts, *Gas-Liquid Reactions*, McGraw-Hill, New York, **1970**.
[13] P. Garstecki, I. Gitlin, W. DiLuzio, G. M. Whitesides, E. Kumacheva, H. A. Stone, *Appl. Phys. Lett.* **2004**, *85*, 2649.
[14] S. L. Kettlewell, A. Schmid, S. Fujii, D. Dupin, S. P. Armes, *Langmuir* **2007**, *23*, 11381.

[15] B. P. Binks, *Curr. Opin. Colloid Interface Sci.* **2002**, *7*, 21.
[16] B. P. Binks, R. Murakami, S. P. Armes, S. Fujii, A. Schmid, *Langmuir* **2007**, *23*, 8691.
[17] F. A. Cotton, G. Wilkinson, *Advanced Inorganic Chemistry*, 4th ed., Wiley, New York, **1980**.
[18] T. Madhavi, A. K. Golder, A. N. Samanta, S. Ray, *Chem. Eng. J.* **2007**, *128*, 95.
[19] X. M. Qi, S. J. Yao, Y. X. Guan, *Biotechnol. Prog.* **2004**, *20*, 1176.
[20] K. Hettiarachchi, E. Talu, M. L. Longo, P. A. Dayton, A. P. Lee, *Lab Chip* **2007**, *7*, 463.
[21] W. Li, E. W. K. Young, M. Seo, Z. Nie, P. Garstecki, C. A. Simmons, E. Kumacheva, *Soft Matter* **2008**, *4*, 258.
[22] T. Nisisako, T. Torii, *Lab Chip* **2008**, *8*, 287.
[23] Y. Xia, G. M. Whitesides, *Angew. Chem.* **1998**, *110*, 568; *Angew. Chem. Int. Ed.* **1998**, *37*, 550.

